Lab on a Chip

Cite this: DOI: 10.1039/c2lc20857a

www.rsc.org/loc

PAPER

Microfluidic biomechanical assay for red blood cells parasitized by *Plasmodium falciparum*

Quan Guo,[a] Sarah J. Reiling,[b] Petra Rohrbach[b] and Hongshen Ma*[acd]

Received 7th September 2011, Accepted 19th December 2011
DOI: 10.1039/c2lc20857a

Red blood cells parasitized by *Plasmodium falciparum* can be distinguished from uninfected cells and characterized on the basis of reduced deformability. To enable improved and simplified analysis, we developed a microfluidic device to measure red blood cell deformability using precisely controlled pressure. Individual red blood cells are deformed through multiple funnel-shaped constrictions with openings ranging from 5 down to 1 μm. Precisely controlled pressures are generated on-chip using a microfluidic circuit that attenuates an externally applied pressure by a factor of 100. The pressures required to squeeze each cell through the constriction are used as a readout to determine the intrinsic stiffness of each cell. Using this method, parasitized cells from ring through schizont stages were shown to be 1.5 to 200 times stiffer than uninfected cells. The measured deformability values of uninfected and parasitized cells showed clearly distinct distributions, demonstrating the potential of using this technique to study the pathophysiology of this disease, and the effect of potential drugs.

Introduction

Malaria is one of the greatest challenges in human health today. Globally, there are 200 to 500 million cases per year, resulting in ~1 million deaths. *Plasmodium falciparum* is the most prevalent causal parasite species, responsible for ~80% of all infections and nearly all mortalities.[1] Central to the pathophysiology of *falciparum* malaria is a reduction in the deformability of infected red blood cells (RBCs), which disrupts normal circulation and causes infected cells to accumulate in the microvasculature of vital organs.[2] The mechanical deformability of parasitized RBCs provides an important biomarker for studying the mechanism of infection and response to treatment, and is therefore important for the development of new drugs.[3] Traditional techniques for studying the biomechanical properties of infected RBCs, including micropipette aspiration,[4–6] optical tweezers,[7–9] and laminar shear flow,[10–13] involve delicate experiments performed by skilled technicians using specialized equipment, and are therefore not readily available for wide-spread use in biological or clinical laboratories.

Microfluidic technologies combine the ability to pattern complex microstructures derived from microfabrication with precise control over the flow of minute volumes of liquid, and thus present new mechanisms for studying cell biomechanics. The integration of such mechanisms in a comprehensive cellular analysis system has the potential to enable accessible, semi-automated, and low-cost experimental diagnostics from a finger-stick blood sample. Recent studies have demonstrated mechanisms to study *P. falciparum* parasitized red blood cells based on capillary obstruction,[14] wedging in tapered constrictions,[15] and transit time through constrictions.[16] These techniques have not been able to produce a sensitive assay to study parasitized RBCs because the readout signals from infected and uninfected cells show broad and overlapping distributions.

In this paper, we introduce a technique for measuring the deformability of red blood cells. Using the threshold pressure required to transit through micrometre-scale constrictions (Fig. 1) as the readout, we show that the deformability of parasitized RBCs could be clearly distinguished from uninfected RBCs, suggesting the potential for deformability-based analysis of parasitized cells without secondary optical verification.

Mechanism and modeling

Our measurement approach involves deforming single RBCs through micrometre scale funnel-shaped constrictions using a precisely controlled hydrodynamic pressure. Each test cell is initially flowed into the mouth of the funnel constriction as shown in Fig. 1. The deformation pressure is then slowly increased until the cell successfully transits through the constriction. The threshold pressure combined with the geometry of the constriction and the volume of the cell is used to calculate the intrinsic stiffness of the cell. A similar approach has been

[a]*Department of Mechanical Engineering, University of British Columbia, 2054-6250 Applied Science Lane, Vancouver, BC, Canada V6T 1Z4. E-mail: hongma@mech.ubc.ca*
[b]*Institute of Parasitology, McGill University, Sainte-Anne-de-Bellevue, QC, Canada*
[c]*Department of Urologic Science, University of British Columbia, Vancouver, BC, Canada*
[d]*Vancouver Prostate Centre, Vancouver General Hospital, Vancouver, BC, Canada*

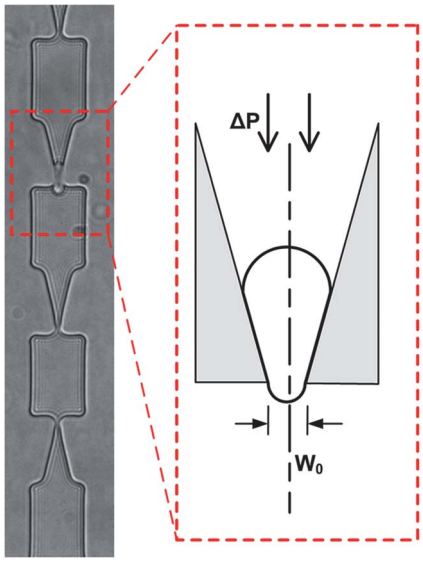

Fig. 1 Red blood cells are individually deformed through micrometre scale funnel constrictions with progressively smaller openings (W_0).

used previously in micropipette aspiration studies.[17,18] In our case, each cell is deformed through several constrictions with progressively smaller openings in order to select a size that presents a measurable deformation pressure. The shape of the funnel constriction is not specifically important for the deformation of RBCs. Instead, the tapered geometry enhances the accuracy and reproducibility of microscale patterns in photolithographic microfabrication, thereby enabling the fabrication of funnel constrictions with precisely controlled openings.

A key difference between our analysis technique and other microfluidic methods, such as capillary obstruction[19] and wedging,[15] is the use of pressure rather than spatial separation to evaluate cell stiffness. Spatial separation is limited by the resolution of microfabrication and optical microscopy, which are both on the order of one micrometre. Pressure measurements, on the other hand, have essentially unlimited resolution, and as a result provide improved capability to discriminate parasitized cells from uninfected cells.

A two-layer microfluidic device[20] was designed to facilitate the process of introducing individual cells into the funnel constriction and then subsequently applying a precisely controlled pressure (Fig. 2). The top layer (flow layer) of this device contains the sample flow channels while the bottom layer (control layer) contains the control microchannels. Three networks of microchannels make up the flow layer: a chain of funnel constrictions, a pressure attenuator, and the cell inlet/outlet. These three microchannels are isolated from one another using valves, S1 through S4, formed at the intersections of flow and control layer microchannels as shown in Fig. 2.

The funnel chain consists of 10 funnel constrictions connected in series with openings of 8, 7, 6, 5, 4, 3, 2.5, 2, 1.5, and 1 μm, and a tapered half angle of 10°. A second chain of 10 funnel constrictions arranged in the mirrored orientation is also connected in series in order to remove any inherent asymmetry in the hydrodynamic resistance of the funnel chain.[21] The height of these funnel constrictions is 3.7 μm in order to constrain normal

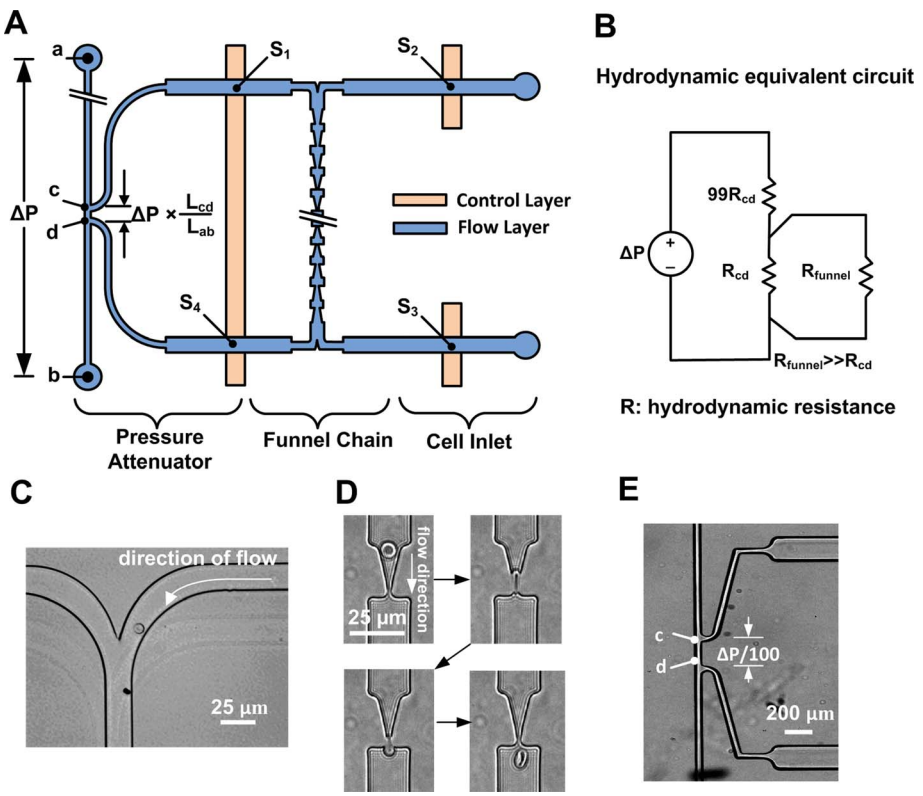

Fig. 2 (A) Design of the flow and control layers of the microfluidic device. (B) Equivalent hydrodynamic circuit of the pressure attenuator. (C–E) Micrographs of the cell inlet, RBC deformation through a funnel constriction, and the pressure attenuator.

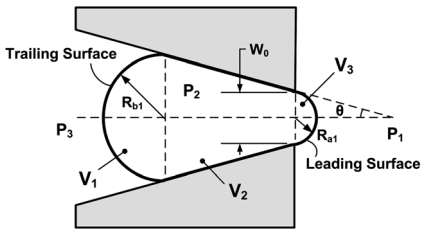

Fig. 3 A geometrical model of a red blood cell being squeezed through the funnel constriction. The cell is pulled rapidly through the constriction by the Haines' jump instability when $R_{a1} = W_0/2$. The value of R_{b1} can be determined in this configuration using volume conservation to relate the threshold deformation pressure with cortical tension of the cell.

RBCs in the planar configuration while allowing the passage of parasitized cells that could take on a more spherical shape.[22] A device height of less than 3.0 μm was found to exclude some RBCs from entering the funnel.

The pressure attenuator divides an externally applied pressure by a factor of 100 and applies this pressure across the funnel chain. This function is accomplished using a fluid equivalent of a resistive divider electronic circuit, which consists of a long microchannel between (a) and (b), and side branches located at (c) and (d), as shown in Fig. 2(A). The distance between (c) and (d) (L_{cd}) is 1/100 of the distance between (a) and (b). As a result, the external pressure applied between (a) and (b) is divided by a factor of 100 as long as the hydrodynamic resistance of the funnel chain is significantly greater than the hydrodynamic resistance between (c) and (d). As a single cell is deformed through a funnel constriction, the flow through the entire funnel chain is blocked. As a result, the pressure applied between (c) and (d) is concentrated across the single constriction that contains the actively deformed cell.

The cell inlet consists of a simple microchannel for introducing single cells into the funnel chain. The measurement process involves first introducing a single cell into the funnel chain *via* the inlet microchannels with valves S1 and S4 closed, and S2 and S3 open. Once a test cell reaches the funnel chain, the states of these valves are inverted, and an attenuated external pressure is applied across the funnel chain to deform the test cell. An earlier version of this microfluidic device was developed to measure the pressure asymmetry between deforming nucleated cells along *versus* against the direction of funnel-shaped microstructures in order to form a microfluidic ratchet mechanism.[23] The pressure asymmetry effect was not observed for RBCs because of their dramatically reduced stiffness.

After the measurement of the threshold pressure, the intrinsic stiffness of each RBC can be determined from a simple model where the cell is considered as a liquid-drop with constant volume and a persistent cortical tension. As each cell is pushed into the funnel, the pressure difference required to quasi-statically form the leading surface, shown in Fig. 3, can be determined using the Laplace–Young equation,[24]

$$P_2 - P_1 = T_c\left(\frac{1}{R_{a1}} + \frac{1}{R_{a2}}\right) \quad (1)$$

where R_{a1} and R_{a2} are the in-plane and out-of-plane radii of curvature, and T_c is the cortical tension of the cell membrane, which describes the intrinsic stiffness of the cell. Similarly, the pressure difference required to form the trailing surface can be determined using

$$P_2 - P_3 = T_c\left(\frac{1}{R_{b1}} + \frac{1}{R_{b2}}\right) \quad (2)$$

where R_{b1} and R_{b2} are the in-plane and out-of-plane radii of curvature of the trailing surface. Subtracting (2) from (1) gives us the expression for ΔP as a function of the principle radii of curvature of the cell,

$$\Delta P = P_3 - P_1 = T_c\left(\frac{1}{R_{a1}} + \frac{1}{R_{a2}} - \frac{1}{R_{b1}} - \frac{1}{R_{b2}}\right) \quad (3)$$

We assume that the deformed RBC conforms to the shape of the funnel constriction, which means that from the planar geometry of the microchannel, the out-of-plane radii of curvature are identical and can be determined by $R_{a2} = R_{b2} = h_{ch}/2$ where h_{ch} is the thickness of the channel. Consequently, eqn (3) simplifies to

$$\Delta P = T_c\left(\frac{1}{R_{a1}} - \frac{1}{R_{b1}}\right) \quad (4)$$

As a cell is pushed into the constriction, the required pressure difference increases until reaching a maximum value, where an instability, known as a Haines' jump,[25] rapidly pulls the cell through the constriction. At the point of instability, $R_{a1} = W_0/2$, and ΔP is the threshold pressure required to squeeze the cell through the funnel constriction.[24] The value of R_b can be calculated using the conservation of volume between the cell in the undeformed state and when it is squeezed into the constriction. Specifically, in the latter case, the deformed cell volume is divided into the volume segments shown in Fig. 3. To reduce the calculation complexity, both V_1 and V_3 are assumed to be semi-discs rather than a more complex three-dimensional shape. The value of R_{b1} can therefore be determined by solving the following equation,

$$\pi R_0^2 h_0 = \left(\frac{1}{2}\pi R_{b1}^2 + \left(R_{b1}^2 - R_{a1}^2\right)\frac{\cos(\theta)}{\sin(\theta)} + \frac{1}{2}\pi R_{a1}^2\right)h_{ch} \quad (5)$$

where R_0 and h_0 are the undeformed diameter and the thickness of the test cell. Once the values for R_{a1} and R_{b1} are known, T_c could then be calculated from the measured threshold pressure using eqn (4).

Materials and methods

Microfabrication

The two-layer microfluidic device consists of a flow layer and a control layer fabricated using multilayer soft-lithography of polydimethylsiloxane (PDMS) silicone.[18] Molds for the flow and control layer microstructures were fabricated separately on silicon wafers. The flow layer consists of two photolithographically defined layers. The funnel chain microstructures were made using an SU-8 3005 photoresist (MicroChem, Newton, MA, USA) thinned with cyclopentanone at a ratio of 1 : 0.8 by volume. The pressure attenuator and cell inlet parts of the mold were made from an SPR 220-7.0 photoresist (MicroChem). The mold for the control layer was made entirely using an SPR

220-7.0 photoresist. The patterns for all three masks were drawn using Solidworks DWG Editor.

The SU-8 3005 part of the flow layer mold was fabricated on a cleaned 100 mm silicon wafer. After dehydration a bake on a hotplate at 200 °C for 5 minutes, the thinned SU-8 3005 was spread onto the wafer at 500 rpm for 10 s, and then spun at 4000 rpm for 30 s. The wafer was then soft baked at 95 °C on the hot plate for 20 minutes before being exposed to UV light in a mask aligner for 30 s. The exposed wafer was given a post-exposure bake in the sequence of 65 °C for 1 minute, 95 °C for 1.5 minutes and then 65 °C for 1 minute. The wafer was then developed using the SU-8 developer (MicroChem). The geometry of the SU-8 photoresist was stabilized by further baking on a hotplate where the bake temperature was gradually ramped from 40 °C to 200 °C, held at 200 °C for one hour, and then gradually cooled to 40 °C.

The SPR part of the flow layer was added to the silicon wafer containing the SU-8 microstructures. An SPR 220-7.0 photoresist was spin-coated on the wafer at 600 rpm for 50 s, and then at 3000 rpm for 2 s to remove the edge-bead. The coated wafer was soft baked on hotplates set at 65 °C for 1 minute, 95 °C for 2 minutes, and then 65 °C for 1 minute. The designed mask for the SPR pattern was then aligned with the SU-8 pattern and exposed for 4 minutes in 30 s bursts. After waiting for approximately 30 min, the wafer was developed using the MF-319 developer (MicroChem). Finally, the developed wafer was annealed for 30 min in a 90 °C oven to create a rounded channel profile. The control layer is made from SPR and fabricated in the same protocol as the SPR part of the flow layer.

Multilayer soft-lithography

Physical replicas of the silicon wafer molds were fabricated using a polyurethane-based plastic (Smooth-Cast 310, Smooth-On) using the process described by Desai *et al.*[26] Microfluidic devices were then fabricated from these molds using multi-layer soft-lithography[18] of RTV615 PDMS (Momentive Performance Material). The flow and control layers were molded separately. To make the flow layer, RTV615 PDMS pre-polymer was poured onto the flow layer mold at a ratio of 5 : 1 base to hardener. The mold with the pre-cured RTV was degassed in a vacuum desiccator for 10 minutes and then baked in the oven for 60 minutes at 65 °C. To make the control layer, the PDMS pre-polymers were mixed at a ratio of 20 : 1 base to hardener, then spin-coated onto a control layer mold at 1800 rpm for 1 minute and then baked in the oven for 50 minutes at 65 °C.

After baking, both partially cured layers were removed from the oven. The flow layer was removed from its mold, and holes were punched into it using a 0.5 mm diameter hole punch (Technical Innovations, Angleton, TX, USA) as the fluidic introduction ports. The flow layer was then aligned and gently pressed facing down onto the control layer. The two-layer device was then baked in the oven for at least 3 hours at 65 °C for diffusion bonding.

After cooling, the bonded device was carefully removed from the control layer mold and the control layer fluidic ports were punched into the double layer device. A standard microscope slide (Fisher Scientific) was cleaned using acetone and isopropanol, and then thoroughly rinsed with DI-H_2O. The double layer device was then bonded to the glass slides by exposing the PDMS control layer side and the glass surface to oxygen plasma (Model PDC-001, Harrick Plasma) for 40 s before the PDMS was brought into contact with the slide to create a permanent covalent bond.

Cell sample preparation

Fresh RBCs. Whole blood was collected with informed consent from healthy donors into 6 ml tubes containing sodium heparin. The tubes were centrifuged at 1000*g* (Clay Adams Serofuge) and washed 3 times with saline. The hematocrit of packed red blood cells was determined using Autocrit Ultra 3 and RBCs were resuspended in Hanks Balances Salt Solution with glucose at 20% or 40% hematocrit as required. Prior to testing with the proposed microfluidic device, 5 µl of the final RBCs sample was diluted in 3 ml of Phosphate Buffer Solution (PBS) with 5% (150 µl) Bovine Serum Albumin (BSA).

***P. falciparum* culture.** The FCB strain of *P. falciparum* parasites was cultured under standard *in vitro* conditions with modifications.[27] Briefly, cultures were maintained at 5% hematocrit in malaria culture medium (1640 RPMI with HEPES; 0.2% sodium bicarbonate; 100 µM hypoxanthine; 10% heat-inactivated human serum; 1 mg ml^{-1} gentamicin). Parasites were incubated in an atmosphere of 5% CO_2, 3% O_2 and 92% N_2 at 37 °C and 95% humidity. Prior to the experiments, blood smears of the cell cultures were prepared. The specimens were air-dried, fixed in methanol and stained with 10% Giemsa to evaluate the stages of the infected cells to be tested. Asynchronous cultures were used to obtain measurements of different parasite stages that were kept under the same conditions. The parasitemia in culture was determined to be 5 to 12%. Prior to the experiments,

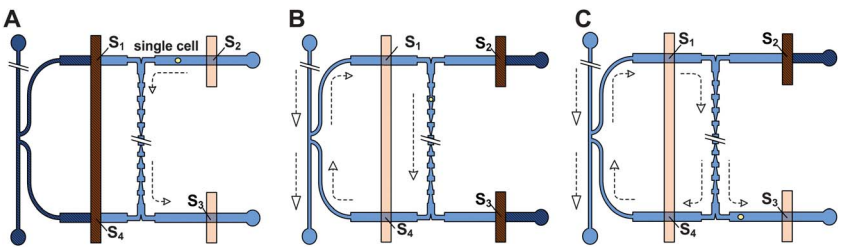

Fig. 4 The sequence of steps used to measure the deformability of single RBCs. (A) A single RBC is infused into the central funnel area with valves S1 and S4 closed, and S2 and S3 open. (B) A precise pressure is applied with S1 and S4 open, and S2 and S3 shut. (C) After each measurement, the test cell is removed by opening S1, S3, and S4.

parasite cultures were centrifuged at 2000 rpm for 5 min. The supernatant was removed and 4 μl of the pellet was resuspended in 3 ml Ringer's solution (122.5 mM NaCl; 5.4 mM KCl; 1.2 mM $CaCl_2 : 2H_2O$; 0.8 mM $MgCl_2 : 6H_2O$; 5.5 mM D-Glucose; 10 mM HEPES; 1 mM $NaH_2PO_4 : H_2O$; pH 7.4) supplemented with 5% BSA.

Experimental apparatus

15 ml conical tubes (Fisher Scientific) containing sample and buffer fluids were sealed with custom-designed caps that act as pressurized reservoirs used to feed fluids into the device. Liquid connections between conical tubes and the PDMS microfluidic device were made using 0.5 mm ID flexible Tygon tubing (Cole-Parmer). The Tygon tubing and the PDMS device were interfaced using 19 mm long 23-gauge stainless steel tubing (New England Small Tube, Litchfield, NH, USA) that formed an elastic, watertight seal on both ends.

Two pneumatic pressure control systems were used to pressurize the reservoirs to infuse fluids into the device. The first system is a custom pressure controller designed to supply pressure from 0 to 4 bar using manual pressure regulators (Omega). The on/off pressure control is enabled using solenoid valves (Pneumadyne) activated by MOSFET switches that are controlled using an MSP430 microcontroller (Texas Instruments) integrated on a printed circuit board. The microcontroller is controlled from a Visual Basic user interface on a PC. The second pressure control system is the MFCS-4C system (Fluigent SA, Paris, France). This system supplies precise pressure with a resolution of 25 mbar (25 Pa) and in the range of 1000 mbar using closed-loop control.

Experimental protocol

The flow channels in the microfluidic device are prepared by dead-end filling using approximately 3 ml Ringer's solution with 5% BSA for the malaria infected RBCs and 3 ml PBS with 5% BSA for fresh RBCs. The device was incubated for 30 minutes to remove air bubbles and prevent non-specific adhesion of the cells to the channel surface. The control channels in the device were filled with DI H_2O.

The process used to measure the threshold pressure required to deform single cells through the funnel constrictions is shown in Fig. 4. A single cell is introduced into the funnel chain network with valves S1 and S4 closed, and S2 and S3 open. Once the cell is present in the funnel chain, S2 and S3 are quickly closed to block the inlets, and S1 and S4 are then opened to apply attenuated pressure. The cell is then manipulated to traverse through the funnel constriction and the critical pressure was determined during this step. After that, the cell is flushed out to the outlet by opening valves S1, S3 and S4.

The process of deforming a single cell going through a funnel constriction is shown in Fig. 2(D). The threshold pressure is measured by gradually increasing the pressure difference across the funnel chain to squeeze the cell through each desired funnel constriction. After passing through a funnel constriction, the cell is then given a few seconds to recover to its original shape before being deformed through a smaller funnel constriction. Each cell is deformed through the same funnel at least three times to determine the average threshold pressure. The deformation pressure in each set of triplicate measurements did not show a downward or upward trend, which suggests that these measurements are not affected by the residual deformation pressure. Therefore, the measured values are deemed valid as long as the cell shows no visible signs of damage and no permanent change in shape.

Results and discussion

To establish the feasibility of our microfluidic cell deformability measurement we first tested the threshold deformation pressures of fresh RBCs collected from healthy donors. For these cells, only the 1.5 and 1.0 μm funnel constrictions showed a measurable deformation pressure. The measured threshold pressures were clustered about a mean value and were consistent and repeatable across different individuals and devices (Fig. 5). The mean deformation pressures were 2.2 and 3.3 Pa for the 1.5 and 1.0 μm constrictions respectively. The mean cortical tension for these fresh, normal RBCs was 2.18 ± 0.23 pN μm^{-1}, which was calculated based on an 8 μm cell diameter and 2.5 μm in thickness.

To evaluate the ability of our technique to discriminate uninfected cells from various stages of parasitized cells, we measured the deformability of *P. falciparum* infected RBCs from *in vitro* cultures. Specifically, we infused asynchronous cell cultures into the device. The threshold pressures are measured for individual cells using one or several constrictions. Each tested RBC was subsequently inspected and identified as uninfected, ring, early trophozoite, mid–late trophozoite, and schizont stages using standard criteria.[28] Briefly, ring stage RBCs contain a faint parasite moving rapidly inside the cell; early trophozoite stage cells contain parasites that begin to lodge at a fixed location; mid–late trophozoite stage cells begin to modify the shape of the RBC by expressing parasite-derived structures and molecules in the RBC cytosol and on the cell surface[29] and show the typical malaria pigment in their digestive vacuole;[30] finally, schizont stage cells contain parasite-derived structures that occupy the majority of the space in the RBC cytosol. Micrographs of parasitized cells from each stage deforming through constrictions

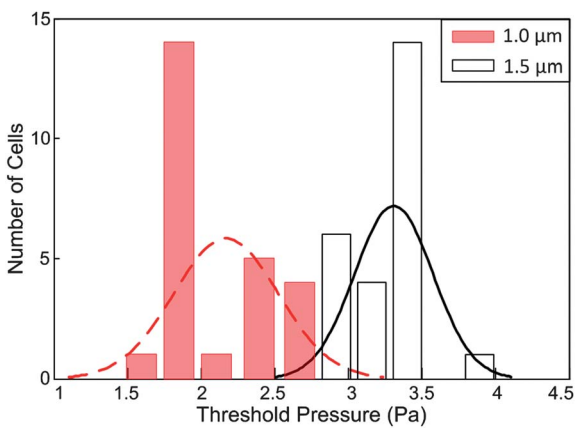

Fig. 5 The threshold pressures required to deform fresh, uninfected red blood cells through 1.5 and 1.0 μm constrictions shown as histograms.

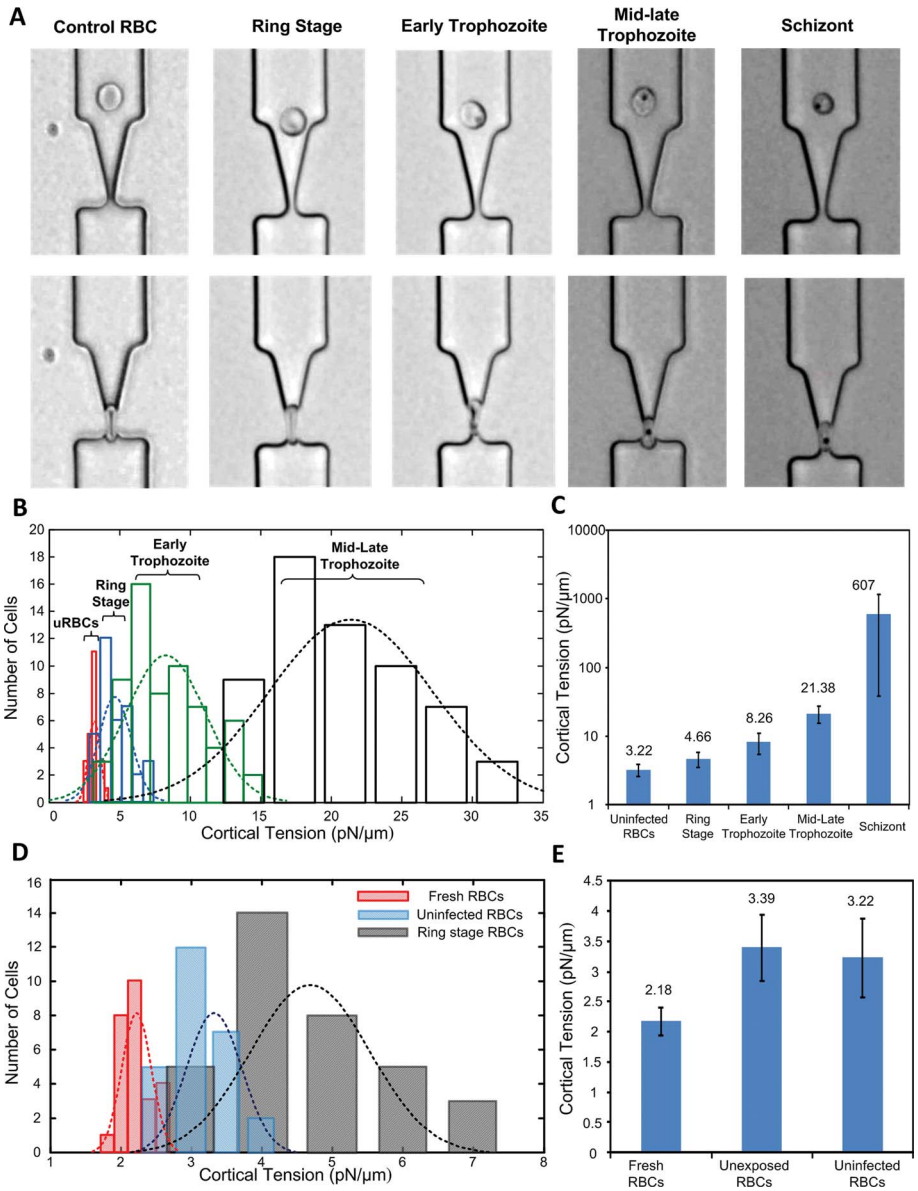

Fig. 6 (A) Micrographs of control and parasitized RBCs being deformed through various funnel constrictions. (B and C) Histogram and bar graph of the measured cortical tension of uninfected RBCs and parasitized RBCs in the ring, early trophozoite, mid–late trophozoite, and schizont stages of infection. (D) Histograms comparing the cortical tension of fresh, uninfected, and ring stage RBCs. (E) Bar graphs comparing the cortical tension of fresh RBCs with 3–4 week old unexposed and uninfected RBCs used to culture the *P. falciparum* parasites.

are shown in Fig. 6(A). At least 25 cells were measured from each stage.

Infected RBCs with ring through mid–late trophozoite stages, along with various types of control cells, were measured using 1.5 and 1.0 μm constrictions. Schizont stages were measured using 5, 4, and/or 3 μm constrictions and were typically obstructed by constrictions less than 3 μm. At this stage, the presence of the parasite dramatically elevates the required deformation pressure. The variation of the cell stiffness is also increased, likely due to the rapid morphological changes associated with the replication and eventual escape of the merozoites from the host cell.

The measured threshold pressures converted to cortical tension of the cell membrane are shown as a histogram in Fig. 6(B) and a bar graph in Fig. 6(C). The results from each stage (except schizont stage) showed an approximately normal distribution with mean and standard deviation values of 3.22 ± 0.64 (uninfected), 4.66 ± 1.15 (rings), 8.26 ± 2.84 (early trophozoites), and 21.38 ± 5.81 (mid–late trophozoites) pN μm^{-1}. The measured cortical tension of schizont stage cells ranges from 85 pN μm^{-1} to 1300 pN μm^{-1}, with an average value of 606 pN μm^{-1}. The loss of RBC deformability associated with the presence and maturity of the parasite is clearly evident and the variation of stiffness associated with different stages is increased in general as the parasite matures, especially for the schizont stage. The ratio of standard deviation over mean, known as the Coefficient of Variation (CV), can be used as a metric for the variability of the measured cell deformability. The CVs for cells at various stages of infection are 0.20

(uninfected RBCs), 0.24 (ring stage), 0.34 (early trophozoite), 0.27 (mid–late trophozoite) and 0.94 (schizont). The significantly greater CV for the schizont stage cells is likely due to the complex morphological changes that modify the cell shape and internal structure. The CV of the deformability of fresh RBCs from healthy donors is 0.10, which is significantly smaller than RBCs used for culture because older RBCs with reduced deformability are actively removed by the human circulatory system.

Compared with previous biomechanical measurements of parasitized RBCs performed using other microfluidic techniques,[15,16,19] as well as micropipette aspiration,[4–6] our technique offers a significantly enhanced signal, along with narrower distributions of the characteristic deformability values associated with each parasite growth stage. Fig. 6(D) shows a detailed histogram comparing the measured cortical tensions of unexposed, uninfected RBCs and ring stage parasitized cells. The mean deformabilities of uninfected and ring stage parasites are clearly separated ($p = 8 \times 10^{-8}$ assessed using the Student's *t*-test). The clear separation between the measured deformabilities of uninfected and various stages of infected cells validates the potential of using deformability measurements to study the properties of parasitized cells and their effect on circulation.

Compared with previous biomechanical measurements of parasitized RBCs performed using optical tweezers,[7,8] our technique measured a dramatically higher relative stiffness for trophozoite and schizont stage parasites, and a lower relative stiffness for ring stage parasites. Specifically, we found trophozoite and schizont stage parasites to be ~7 and ~200 times stiffer than uninfected cells, whereas optical tweezer studies found these cells to be ~4 and ~10 times stiffer, respectively. Conversely, we found ring stage parasites to be ~1.5 times stiffer than uninfected cells, whereas optical tweezer studies found these cells to be ~3 times stiffer. These differences likely stem from the nature of the mechanical constraint associated with each measurement. Optical tweezer studies measure the resistance to tensile stretching applied to microbeads attached to two points on the cell surface, where the restoring force is solely provided by the cell membrane. Our microfluidic technique deforms the test cell in compression without tangential constraint, where the restoring force is provided by the cytoplasm and the membrane. In ring stage parasites, the dominant stiffening mechanism is the modification of the cell membrane caused by proteins exported by the parasite.[9] Therefore, a greater mechanical change is measured using optical tweezers. In trophozoite and schizont stage parasites, the dominant stiffening mechanism is the presence of parasite-derived structures in the cytosol. Consequently, a greater mechanical change is measured using our technique. For biophysical studies, our technique provides a measure of the stiffness of parasitized RBCs that more closely resembles the mechanics of circulation and blood vessel occlusion.

The RBCs used to culture the *P. falciparum* parasites were approximately 3–4 weeks old. To study the cell stiffening associated with aging, we measured the stiffness of RBCs used to culture the parasite before and after exposure to the parasite. As expected, the cells used for culture were stiffer than fresh RBCs.[31] The increase in stiffness due to aging was approximately 50% (Fig. 6(E)). We did not observe a statistically significant difference between the unexposed and exposed uninfected RBCs, which suggests that the presence of *P. falciparum* proteins in the cell culture medium does not change the stiffness of uninfected RBCs. Our finding contradicts the results previously obtained using optical tweezers.[7,8]

Finally, it is interesting to note that the deformability distributions from all stages of infected RBCs show a slight skew towards values smaller than the mean. This characteristic is consistent with the deformability distribution of uninfected RBCs found in the parasite culture, which shows a similar type of skew (Fig. 6(D)). While *P. falciparum* parasites are grown in culture, the deformabilities of both infected and uninfected RBCs are gradually reduced because of aging. This degradation process is likely to have a non-uniform effect on RBC deformability producing a skewed distribution. The deformability distribution of infected cells is therefore a convolution of the deformability distribution of the uninfected RBCs and the loss of deformability resulting from the infection.

Conclusion

In summary, we developed a microfluidic technique for measuring the deformability of single RBCs based on their ability to deform through micrometre-scale constrictions. Using the threshold deformation pressure as the readout signal, we showed that the characteristic deformability distributions of uninfected RBCs and RBCs with various stages of *P. falciparum* infection are clearly distinct from one another, indicating the potential of using this technique to identify the infected cells without secondary visual verification to study the properties of infected cells and their response to treatment.

Acknowledgements

The authors would like to thank Mark Scott and Dana Kyluik for providing materials used in this study, and Sarah McFaul, Lily So, and Jacky Chan for technical assistance. This work was supported by grants from the Bill and Melinda Gates Foundation, Natural Science and Engineering Research Council of Canada, Canadian Institutes of Health Research, Michael Smith Foundation for Health Research, Genome British Columbia, Burroughs Wellcome Fund, and the PC-TRIADD Centre of Excellence in Research and Commercialization at the Vancouver Prostate Centre.

References

1 R. Tuteja, *FEBS J.*, 2007, **274**, 4670–4679.
2 A. M. Dondorp, P. A. Kager, J. Vreeken and N. J. White, *Parasitol. Today*, 2000, **16**, 228–232.
3 M. Diez-Silva, M. Dao, J. Y. Han, C. T. Lim and S. Suresh, *MRS Bull.*, 2010, **35**, 382–388.
4 G. B. Nash, E. Obrien, E. C. Gordonsmith and J. A. Dormandy, *Blood*, 1989, **74**, 855–861.
5 F. K. Glenister, R. L. Coppel, A. F. Cowman, N. Mohandas and B. M. Cooke, *Blood*, 2002, **99**, 1060–1063.
6 M. Paulitschke and G. B. Nash, *J. Lab. Clin. Med.*, 1993, **122**, 581–589.
7 J. P. Mills, L. Qie, M. Dao, K. S. W. Tan, C. T. Lim and S. Suresh, in *Mater Res Soc Symp Proc*, ed. C. Viney, K. Katti, F. J. Ulm and C. Hellmich, Materials Research Society, Warrendale, 2005, pp. 179–184.
8 S. Suresh, J. Spatz, J. P. Mills, A. Micoulet, M. Dao, C. T. Lim, M. Beil and T. Seufferlein, *Acta Biomater.*, 2005, **1**, 15–30.

9 J. P. Mills, M. Diez-Silva, D. J. Quinn, M. Dao, M. J. Lang, K. S. W. Tan, C. T. Lim, G. Milon, P. H. David, O. Mercereau-Puijalon, S. Bonnefoy and S. Suresh, *Proc. Natl. Acad. Sci. U. S. A.*, 2007, **104**, 9213–9217.
10 H. A. Cranston, C. W. Boylan, G. L. Carroll, S. P. Sutera, J. R. Williamson, I. Y. Gluzman and D. J. Krogstad, *Science*, 1984, **223**, 400–403.
11 L. H. Miller, S. Usami and S. Chien, *J. Clin. Invest.*, 1971, **50**, 1451–1455.
12 L. H. Miller, S. Usami and S. Chien, *Am. J. Trop. Med. Hyg.*, 1972, **21**, 133–137.
13 R. Suwanarusk, B. M. Cooke, A. M. Dondorp, K. Silamut, J. Sattabongkot, N. J. White and R. Udomsangpetch, *J. Infect. Dis.*, 2004, **189**, 190–194.
14 J. P. Shelby, J. White, K. Ganesan, P. K. Rathod and D. T. Chiu, *Proc. Natl. Acad. Sci. U. S. A.*, 2003, **100**, 14618–14622.
15 T. Herricks, M. Antia and P. K. Rathod, *Cell. Microbiol.*, 2009, **11**, 1340–1353.
16 H. Bow, I. V. Pivkin, M. Diez-Silva, S. J. Goldfless, M. Dao, J. C. Niles, S. Suresh and J. Y. Han, *Lab Chip*, 2011, **11**, 1065–1073.
17 E. Evans and B. Kukan, *Blood*, 1984, **64**, 1028–1035.
18 E. A. Evans and R. M. Hochmuth, *Biophys. J.*, 1976, **16**, 1–11.
19 J. P. Shelby, J. White, K. Ganesan, P. K. Rathod and D. T. Chiu, *Proc. Natl. Acad. Sci. U. S. A.*, 2003, **100**, 14618–14622.
20 M. A. Unger, H. P. Chou, T. Thorsen, A. Scherer and S. R. Quake, *Science*, 2000, **288**, 113–116.
21 A. Groisman and S. R. Quake, *Phys. Rev. Lett.*, 2004, **92**, 094501.
22 A. Esposito, J. B. Choimet, J. N. Skepper, J. M. A. Mauritz, V. L. Lew, C. F. Kaminski and T. Tiffert, *Biophys. J.*, 2010, **99**, 953–960.
23 Q. Guo, S. M. McFaul and H. Ma, *Phys. Rev. E*, 2011, **83**, 051910.
24 R. M. Hochmuth, *J. Biomech.*, 2000, **33**, 15–22.
25 W. B. Haines, *J. Agric. Sci.*, 1930, **20**, 97–116.
26 S. P. Desai, D. M. Freeman and J. Voldman, *Lab Chip*, 2009, **9**, 1631–1637.
27 W. Trager and J. B. Jensen, *Science*, 1976, **193**, 673–675.
28 G. Coatney, W. Collins, M. Warren and P. Contacos, *The Primate Malarias*, U.S. Department of Health, Education and Welfare, Bethesda, 1971.
29 E. Knuepfer, M. Rug, N. Klonis, L. Tilley and A. F. Cowman, *Blood*, 2005, **105**, 4078–4087.
30 S. G. Langreth, J. B. Jensen, R. T. Reese and W. Trager, *J. Protozool.*, 1978, **25**, 443–452.
31 M. Marinkovic, M. Diez-Silva, I. Pantic, J. J. Fredberg, S. Suresh and J. P. Butler, *Am. J. Physiol.: Cell Physiol.*, 2009, **296**, C59–C64.